Available online at www.sciencedirect.com

ScienceDirect

Ceramics International 40 (2014) 1729–1733

CERAMICS INTERNATIONAL

www.elsevier.com/locate/ceramint

Improved photocatalytic and gas sensing properties of α-Fe_2O_3 nanoparticles derived from β-FeOOH nanospindles

Hui Yan[a], Xintai Su[a,*], Chao Yang[a], Jide Wang[a], Chunge Niu[b]

[a]Ministry Key Laboratory of Oil and Gas Fine Chemicals, College of Chemistry and Chemical Engineering, Xinjiang University, Urumqi 830046, China
[b]Petrochemical Research Institute, Karamay Petrochemical Company, Karamay, Xinjiang 83400, China

Received 27 April 2013; received in revised form 8 July 2013; accepted 15 July 2013
Available online 22 July 2013

Abstract

α-Fe_2O_3 nanoparticles were synthesized through calcining the as-synthesized spindle-like β-FeOOH precursors at 600 °C. X-ray powder diffraction (XRD) and transmission electron microscopy (TEM) results showed that β-FeOOH nanospindles with a diameter of ~50 nm and lengths up to 100–150 nm were readily changed to α-Fe_2O_3 nanoparticles with a size of 30–150 nm after heat-treatment for 2 h. The photocatalytic performances of the as-prepared samples were evaluated by photocatalytic decolorization of methylene blue (MB) in the presence of H_2O_2 at ambient temperature. The results indicated that the α-Fe_2O_3 nanoparticles exhibited the highest photocatalytic activity compared with the β-FeOOH nanospindles and the commercial α-Fe_2O_3 powders. The gas-sensing measurement results demonstrated that the products showed an excellent gas response to ethanol and acetone. The results showed that these α-Fe_2O_3 nanoparticles may have potential applications in gas sensor and photocatalysts.

Keywords: E. Sensors; β-FeOOH; α-Fe_2O_3; Nanoparticles; Photocatalysts

1. Introduction

Hematite (α-Fe_2O_3) is the most thermodynamically stable iron oxide with n-type semiconducting properties (E_g = 2.1 eV) under ambient conditions. It has been extensively used in many fields, such as magnetics [1,2], catalysts [3,4], gas-sensing [5,6], pigments [7] and water treatment [8,9], as well as in other biological and medical fields due to its low cost, environmental friendliness, and fascinating physicochemical properties. Nanostructured materials are expected to have improved physicochemical properties compared with bulk materials due to their size effects, large surface area to volume ratios and possible quantum confinement effects [10].

Many efforts have been directed to fabricate α-Fe_2O_3 nanostructures with specific size and morphology [11–13] because of their unique electrical, optical and magnetic properties for the potential applications in a lot of fields. Stimulated by these intriguing properties and extensive applications, a variety of methods have been reported for the synthesis of α-Fe_2O_3 nanostructures, including the vapor–solid growth method, sol–gel approach, hydrothermal technique and the chemical precipitation process. Zhonglin Wang groups have synthesized uniform α-Fe_2O_3 nanowire arrays by a vapor–solid method, and systematically studied the growth machanism of the α-Fe_2O_3 aligned arrays [14]. Wael Hamd et al. fabricated α-Fe_2O_3 mesoporous films by a template-directed sol–gel method combined with a dip-coating approach and followed by annealing at various temperatures in air [15]. Guohong Qiu et al. have synthesized nanosized α-Fe_2O_3 powder by a microwave-assisted hydrothermal reaction of $Fe(NO_3)_3$ in the presence of urea at 120 °C [16]. Although there are a lot of successes in the synthesis of α-Fe_2O_3 nanostructures, a facile method is still required.

Herein, α-Fe_2O_3 nanoparticles are prepared by a combined method of hydrolysis and calcination. The hydrolysis of $FeCl_3$ solution gives uniformly sized β-FeOOH nanospindles that serve as the precursor for α-Fe_2O_3 nanoparticles. Despite the size and shape changes, the calcination-derived α-Fe_2O_3 nanoparticles show phase pure hematite and high crystallinity. Moreover, the well-defined β-FeOOH precursor may provide a natural defense from the heavy agglomeration of α-Fe_2O_3

*Corresponding author. Tel./fax: +86 991 8582335.
E-mail address: suxintai827@163.com (X. Su).

0272-8842/$ - see front matter © 2013 Elsevier Ltd and Techna Group S.r.l. All rights reserved.
http://dx.doi.org/10.1016/j.ceramint.2013.07.070

nanoparticles, resulting in network-like nanoparticle aggregates. These networks should have an effective contact surface area and accessible defuse pathway for the molecule adsorption and desorption. It is thus expected that the as-synthesized α-Fe_2O_3 nanoparticles show high photo-catalytic activity and gas-sensing performance. The visible light photo-degradation of MB on the synthesized α-Fe_2O_3 nanoparticles shows their obviously higher ability than that of the β-FeOOH precursor. Furthermore, the gas-sensing measurements of the synthesized α-Fe_2O_3 nanoparticles exhibit an excellent ethanol- and acetone-sensing performance.

2. Experimental

2.1. Sample preparation

All the reagents used in the experiment were analytical grade without further purification. The precursor β-FeOOH was obtained from hydrolysis of diluted aqueous iron chloride ($FeCl_3 \cdot 6H_2O$) solution. In a typical process, 0.02 mol L^{-1} aqueous solution of $FeCl_3$ was heated at 80 °C for 24 h under magnetic stirring. After cooling to room temperature, the product was washed with deionized water and ethanol for several times, and then dried at 40 °C in air for 8 h. After that, the as-obtained β-FeOOH was heated in air at 600 °C for 2 h to obtain the α-Fe_2O_3.

2.2. Characterization

The phase and crystallinity of the obtained samples were characterized by XRD using a Bruker D8 advanced X-ray diffractometer with Cu Kα radiation ($\lambda = 1.54056$ Å). The 2θ range used was from 10° to 80°. TEM images were obtained on a Hitachi H-600 with an accelerating voltage of 100 kV.

2.3. Photocatalytic experiment

The photocatalytic experiment was carried out in an equipment of XPA-7 (G8) photochemical action instrument (Xujiang Electromechanical plant, Nanjing, China). A 350 W Xe lamp was used as a light source with cutoff filter (< 420 nm). In a typical process, aqueous suspensions of MB (50 mL, 10 mg L^{-1}) and 10 mg of samples were mixed into a quartz tube. Prior to irradiation, the solution was continuously stirred for 30 min in the dark to ensure the establishment of an adsorption–desorption equilibrium. Then 100 μL H_2O_2 (30% aqueous solution) was added into the solution. The UV–vis spectrophotometer (Shimadzu UV-2450 PC) was used to monitor the concentration of MB during the photodegradation. The percentage of photodegradation is reported as C/C_0, where C is the concentration of MB for each irradiated time, and C_0 is the starting concentration.

2.4. Sensor fabrication

The method and instrument of the gas sensing test were similar to that of our previous work [17]. The as-synthesized sensor was fixed into the gas sensing apparatus and aged at 300 °C for 48 h. Gas sensing measurements were carried out on a computer-controlled WS-30A system (Zhengzhou, China). Here, the gas response is defined as R_a/R_g, where R_a and R_g are the resistance of the sensor in clean air and in detected gas, respectively.

3. Results and discussion

3.1. Structure characterization

Fig. 1 shows the XRD patterns of the precursor and the as-synthesized sample. Fig. 1a exhibits the precursor fabricated by the hydrolysis of iron chloride solution. It is obvious that almost all the reflections can be readily indexed to a tetragonal β-FeOOH phase (JCPDS no. 34-1266). A complete conversion from β-FeOOH to α-Fe_2O_3 is achieved by the calcination of the spindle-shaped β-FeOOH, which can be proved by the XRD pattern in Fig. 1b. The product shows a hexagonal structure of α-Fe_2O_3 (JCPDS no. 33-0664, (a) 5.035 Å, (b) 5.535 Å and (c) 13.74 Å).

The morphologies of the obtained precursor and product were characterized by TEM. Fig. 2a shows the TEM image of the β-FeOOH precursor that exhibits a regular spindle shape with diameter of about 50 nm and length of about 100–150 nm. Furthermore, the spindle-shaped β-FeOOH completely transformed to α-Fe_2O_3 nanoparticles after heated at 600 °C for 2 h, as shown in Fig. 2b. Interestingly, the morphology of the α-Fe_2O_3 nanoparticles is irregular particle with a size of about 30–150 nm.

3.2. Photocatalytic experiment

The visible-light photocatalytic activity of the β-FeOOH, the commercial α-Fe_2O_3 and the as-prepared α-Fe_2O_3 nanoparticles was evaluated by the degradation of MB solution. Fig. 3a gives the evolution of the MB absorption spectra in the

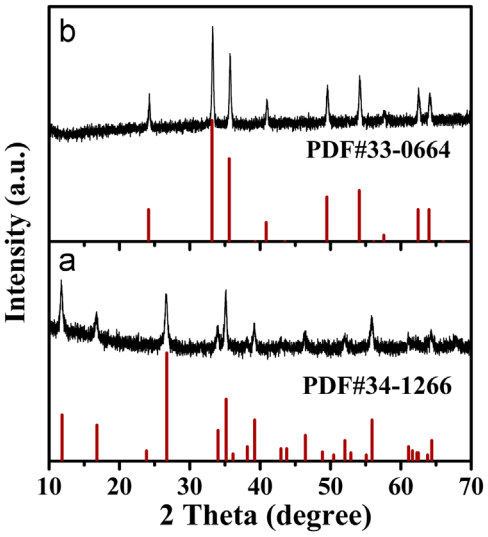

Fig. 1. Powder XRD patterns of β-FeOOH precursor (a) and α-Fe_2O_3 nanoparticles (b).

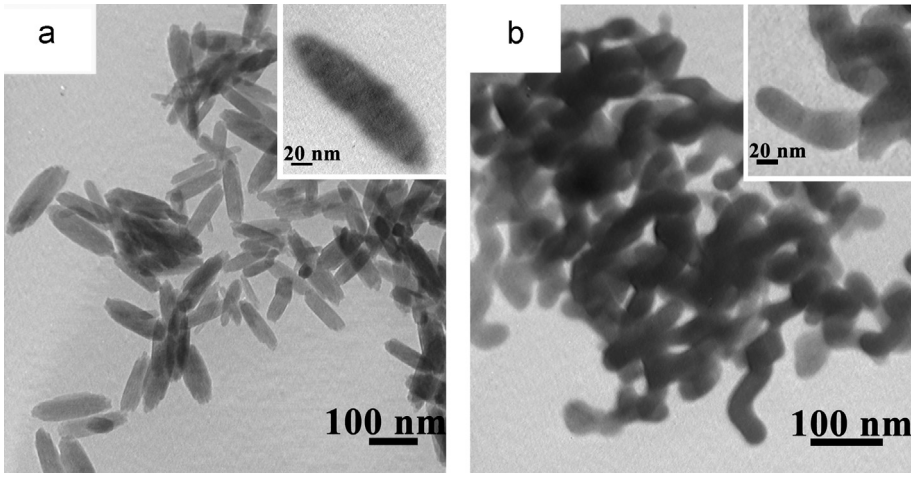

Fig. 2. TEM images of β-FeOOH precursor (a) and α-Fe_2O_3 nanoparticles (b).

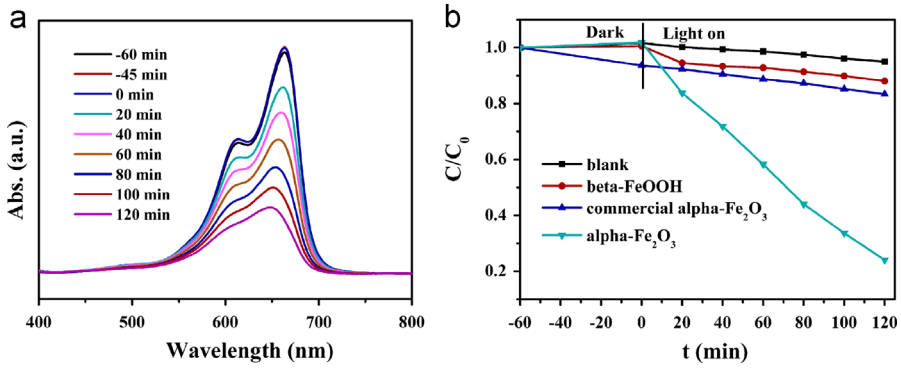

Fig. 3. (a) UV/vis spectroscopic changes of the MB aqueous solution in the presence of α-Fe_2O_3 nanoparticles and H_2O_2; (b) the change of MB concentration over various iron oxides as a function of irradiation time. The blank one is photolysis in the presence of H_2O_2 only.

presence of α-Fe_2O_3 nanoparticles as a function of time under visible light irradiation ($\lambda > 420$ nm). The intensity of the characteristic peak of MB at $\lambda = 663.5$ nm was found to decrease gradually with prolong irradiation time, showing its effective photodegradation of MB. Fig. 3b shows a plot of the photodegradation extent of the MB molecules with the increase of the irradiation time for the β-FeOOH, the commercial α-Fe_2O_3 and the α-Fe_2O_3 nanoparticles in the presence of H_2O_2 at ambient temperature. It can be seen that the degradation of MB molecules by the α-Fe_2O_3 nanoparticles is fast and approaches to 80% within 120 min. As comparison, a negligible degradation of MB is found in the absence of the α-Fe_2O_3 nanoparticles or in the presence of the β-FeOOH precursor (Fig. 3b). The commercial α-Fe_2O_3 shows a certain adsorption performance. However, the photocatalytic property is much lower than that of the α-Fe_2O_3 nanoparticles.

3.3. Gas-sensing performance

As is well-known, the response of a semiconductor gas sensor is highly affected by its operating temperature. In order to determine the optimum operating temperature, the response of the α-Fe_2O_3 sensor to 100 ppm ethanol at different operating temperatures was tested, as shown in Fig. 4. It is obvious that the response increased

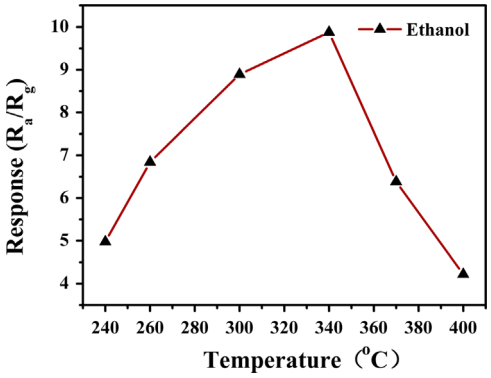

Fig. 4. Response of the α-Fe_2O_3-based sensor to 100 ppm ethanol as a function of operating temperature.

with temperature, reached the maximum value at 340 °C, and decreased further with prolong temperature. The phenomenon can be explained by the following. With the increase of operating temperature, the amount of gas adsorbed becomes high and the adsorption attains a balance at a suitable temperature (namely optimum temperature). However, the amount of gas adsorbed will reduce when the operating temperature keeps on increasing, and the balance will change to desorption, leading to a decreased gas

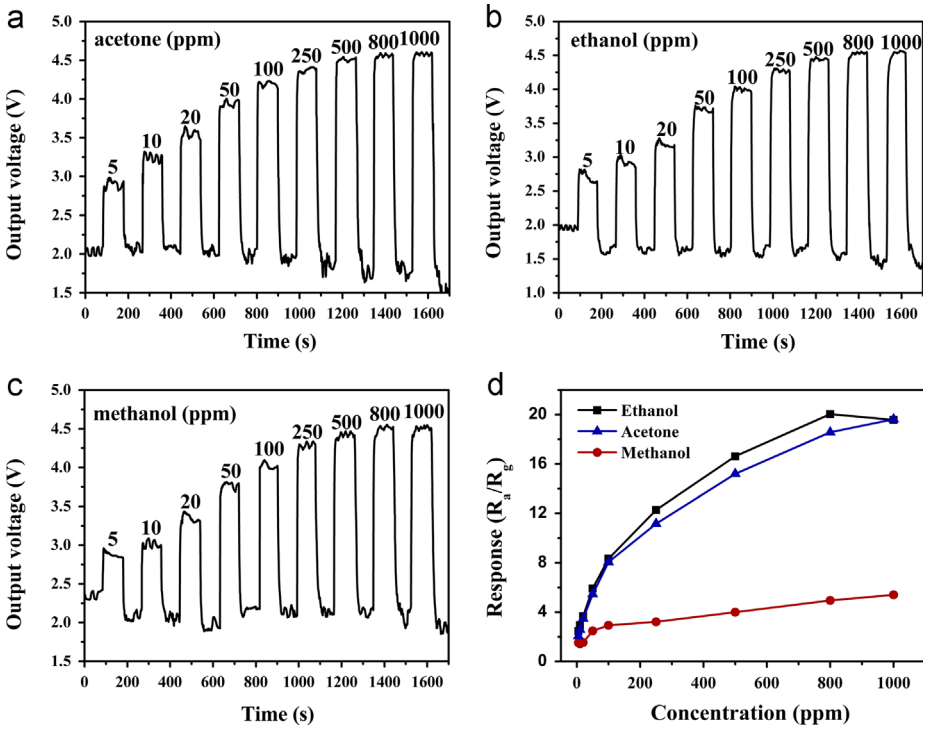

Fig. 5. Typical response–recovery curves of the α-Fe_2O_3-based sensor to various concentrations of acetone (a), ethanol (b) and methanol (c) at the operating temperature of 340 °C. (d) Response of the sensor to different ethanol, acetone and methanol concentrations.

sensitivity when the operating temperature exceeds the optimum values [18]. The maximum response reached 10 toward 100 ppm ethanol at 340 °C. Therefore, the optimal operating temperature was fixed at 340 °C for the subsequent gas detections.

The response and recovery behavior were further investigated with the α-Fe_2O_3-based sensor exposed to ethanol, acetone and methanol at different concentrations at 340 °C, respectively, as shown in Fig. 5(a–c). It can be seen that the output voltage increases suddenly on the injection of the tested gas, and then decreases rapidly to the initial value after exposure to air, which indicates that the α-Fe_2O_3-based sensor has good reversibility. Fig. 5(d) illustrates the response defined as R_a/R_g to ethanol, acetone and methanol, respectively. With the increase in the gas concentration, the response greatly increased. The response values of the α-Fe_2O_3-based sensor to ethanol and acetone were 2.94 and 2.58, respectively, even at low concentration of 10 ppm, indicating that the sensor has good gas-sensing properties.

4. Conclusions

In conclusion, α-Fe_2O_3 nanoparticles were prepared through annealing the β-FeOOH precursor obtained from hydrolysis of $FeCl_3 \cdot 6H_2O$. Moreover, the gas sensing property and the photocatalytic activity of the synthesized products were evaluated. The results showed that the α-Fe_2O_3 nanoparticles exhibited excellent photocatalytic properties towards MB and high gas response to ethanol and acetone, suggesting that these products may have potential applications in the field of photocatalysis and gas sensors.

Acknowledgments

We appreciate the financial supports of NSFC (21266031), Scientific and Technological Assistance Projects in Xinjiang (201191102) and International Cooperation Projects in Xinjiang (20116011).

References

[1] B. Wang, J.S. Chen, H.B. Wu, Z. Wang, X.W. Lou, Quasiemulsion-templated formation of α-Fe_2O_3 hollow spheres with enhanced lithium storage properties, Journal of the American Chemical Society 133 (2011) 17146–17148.

[2] J. Ma, J. Lian, X. Duan, X. Liu, W. Zheng, α-Fe_2O_3: hydrothermal synthesis, magnetic and electrochemical properties, The Journal of Physical Chemistry C 114 (2010) 10671–10676.

[3] S. Yang, Y. Xu, Y. Sun, G. Zhang, D. Gao, Size-controlled synthesis, magnetic property, and photocatalytic property of uniform α-Fe_2O_3 nanoparticles via a facile additive-free hydrothermal route, CrystEngComm 14 (2012) 7915–7921.

[4] J. Ma, J. Teo, L. Mei, Z. Zhong, Q. Li, T. Wang, X. Duan, J. Lian, W. Zheng, Porous platelike hematite mesocrystals: synthesis, catalytic and gas-sensing applications, Journal of Materials Chemistry 22 (2012) 11694–11700.

[5] Y. Wang, J. Cao, S. Wang, X. Guo, J. Zhang, H. Xia, S. Zhang, S. Wu, Facile synthesis of porous α-Fe_2O_3 nanorods and their application in ethanol sensors, The Journal of Physical Chemistry C 112 (2008) 17804–17808.

[6] B. Sun, J. Horvat, H.S. Kim, W.S. Kim, J. Ahn, G. Wang, Synthesis of mesoporous α-Fe_2O_3 nanostructures for highly sensitive gas sensors and high capacity anode materials in lithium ion batteries, The Journal of Physical Chemistry C 114 (2010) 18753–18761.

[7] X. Zhou, J. Lan, G. Liu, K. Deng, Y. Yang, G. Nie, J. Yu, L. Zhi, Facet-mediated photodegradation of organic dye over hematite architectures by visible light, Angewandte Chemie 124 (2012) 182–186.

[8] Z. Wei, R. Xing, X. Zhang, S. Liu, H. Yu, P. Li, Facile Template-free fabrication of hollow nestlike α-Fe_2O_3 nanostructures for water treatment, ACS Applied Materials and Interfaces 5 (2013) 598–604.
[9] X.L. Fang, C. Chen, M.S. Jin, Q. Kuang, Z.X. Xie, S.Y. Xie, R. B. Huang, L.S. Zheng, Single-crystal-like hematite colloidal nanocrystal clusters: synthesis and applications in gas sensors, photocatalysis and water treatment, Journal of Materials Chemistry 19 (2009) 6154–6160.
[10] C. Burda, X. Chen, R. Narayanan, M.A. El-Sayed, Chemistry and properties of nanocrystals of different shapes, Chemical Reviews-Columbus 105 (2005) 1025–1102.
[11] A.G. Nasibulin, S. Rackauskas, H. Jiang, Y. Tian, P.R. Mudimela, S. D. Shandakov, L.I. Nasibulina, S. Jani, E.I. Kauppinen, Simple and rapid synthesis of α-Fe_2O_3 nanowires under ambient conditions, Nano Research 2 (2009) 373–379.
[12] F. Song, J. Guan, X. Fan, G. Yan, Single-crystal star-like arrayed particles of hematite: synthesis, formation mechanism and magnetic properties, Journal of Alloys and Compounds 485 (2009) 753–758.
[13] C.Y. Cao, J. Qu, W.-S. Yan, J.F. Zhu, Z.Y. Wu, W.G. Song, Low-cost synthesis of flowerlike α-Fe_2O_3 nanostructures for heavy metal ion removal: adsorption property and mechanism, Langmuir 28 (2012) 4573–4579.
[14] Y.L. Chueh, M.W. Lai, J.Q. Liang, L.J. Chou, Z.L. Wang, Systematic study of the growth of aligned arrays of α-Fe_2O_3 and Fe_3O_4 nanowires by a vapor–solid process, Advanced Functional Materials 16 (2006) 2243–2251.
[15] W. Hamd, S. Cobo, J. Fize, G. Baldinozzi, W. Schwartz, M. Reymermier, A. Pereira, M. Fontecave, V. Artero, C. Laberty-Robert, Mesoporous α-Fe_2O_3 thin films synthesized via the sol–gel process for light-driven water oxidation, Physical Chemistry Chemical Physics 14 (2012) 13224–13232.
[16] G. Qiu, H. Huang, H. Genuino, N. Opembe, L. Stafford, S. Dharmarathna, S.L. Suib, Microwave-assisted hydrothermal synthesis of nanosized α-Fe_2O_3 for catalysts and adsorbents, The Journal of Physical Chemistry C 115 (2011) 19626–19631.
[17] C. Yang, X. Su, F. Xiao, J. Jian, J. Wang, Gas sensing properties of CuO nanorods synthesized by a microwave-assisted hydrothermal method, Sensors and Actuators B: Chemical 158 (2011) 299–303.
[18] J. Xu, X. Jia, X. Lou, G. Xi, J. Han, Q. Gao, Selective detection of HCHO gas using mixed oxides of ZnO/$ZnSnO_3$, Sensors and Actuators B: Chemical 120 (2007) 694–699.